water

MDPI

Article

Multiscale Spatiotemporal Dynamics of Drought within the Yellow River Basin (YRB): An Examination of Regional Variability and Trends

Lei Jin, Shaodan Chen * and Mengfan Liu

School of Water Conservancy and Transportation, Zhengzhou University, Zhengzhou 450001, China; jinlei@gs.zzu.edu.cn (L.J.); liumf@gs.zzu.edu.cn (M.L.)
* Correspondence: chensd@zzu.edu.cn

Abstract: Drought, as a recurring extreme climatic event, inflicts diverse impacts on ecological systems, agricultural productivity, water resources, and socio-economic progress globally. Discerning the drought patterns within the evolving environmental landscape of the Yellow River Basin (YRB) is imperative for enhancing regional drought management and fostering ecological conservation alongside high-quality development. This study utilizes meteorological drought indices, the Standardized Precipitation Evapotranspiration Index (SPEI) and the self-calibrating Palmer Drought Severity Index (scPDSI), for a detailed spatiotemporal analysis of drought conditions. It examines the effectiveness of these indices in the basin's drought monitoring, offering a comprehensive insight into the area's drought spatiotemporal dynamics. The findings demonstrate the following: (1) SPEI values exhibit distinct fluctuation patterns at varying temporal scales, with more pronounced fluctuations at shorter scales. Drought years identified via the 12-month SPEI time scale include 1965, 1966, 1969, 1972, 1986, 1997, 1999, 2001, and 2006. (2) A modified Mann–Kendall (MMK) trend test analysis of the scPDSI time series reveals a worrying trend of intensifying drought conditions within the basin. (3) Correlation analysis between SPEI and scPDSI across different time scales yields correlation coefficients of 0.35, 0.54, 0.69, 0.76, and 0.62, highlighting the most substantial correlation at an annual scale. Spatial correlation analysis conducted between SPEI and scPDSI across various scales reveals that, within diverse temporal ranges, the correlation peaks at a 12-month time scale, with subsequent prominence observed at 6 and 24 months. This observed pattern accentuates the applicability of scPDSI in the monitoring of medium- to long-term drought phenomena.

Keywords: meteorological drought; SPEI; scPDSI; Yellow River Basin (YRB)

Citation: Jin, L.; Chen, S.; Liu, M. Multiscale Spatiotemporal Dynamics of Drought within the Yellow River Basin (YRB): An Examination of Regional Variability and Trends. *Water* **2024**, *16*, 791. https://doi.org/10.3390/w16050791

Academic Editor: Thomas C. Piechota

Received: 4 February 2024
Revised: 21 February 2024
Accepted: 3 March 2024
Published: 6 March 2024

1. Introduction

Drought, a pervasive and recurrent natural hazard, profoundly impacts diverse facets of human endeavors globally [1,2]. The Intergovernmental Panel on Climate Change, in its Sixth Assessment Report, emphasizes that climate change is intensifying drought conditions worldwide through elevated temperatures and shifting precipitation patterns [3]. Particularly, in China, drought emerges primarily due to inadequate precipitation, amongst other contributing elements. Drought's hallmark characteristics include its high frequency, prolonged duration, and extensive impacts. It represents a cumulative process where a persistent deficit in regional surface water, primarily influenced by precipitation and evapotranspiration, takes a central role amidst various meteorological factors [4,5]. The frequent and enduring nature of drought not only precipitates significant economic losses but also triggers a cascade of adverse effects such as acute water shortages, accelerated land desertification, and an increased incidence of sandstorms and dust storms [6–8]. Consequently, timely and precise drought monitoring is imperative for the judicious management of regional water resources, bolstering socio-economic progress, and fostering the sustainable development of the ecological environment.

Drought manifests in four principal forms: socioeconomic, agricultural, hydrological, and meteorological. Typically, the onset of other drought types is heralded by a meteorological drought, which usually precedes them [9–11]. Typically, a diminution in precipitation precipitates the onset of a meteorological drought. This sequence of events invariably leads to a reduction in soil moisture levels, thereby impeding the effective irrigation of crops and consequently instigating agricultural drought due to diminished crop yields. When it progresses to a certain stage, such conditions can culminate in a decrease in river flows or reservoir storage levels, thereby triggering a hydrological drought. These cascading effects extend to the socio-economic realm, where the fundamental water requirements of society and the economy are unmet, ultimately resulting in a socio-economic drought characterized by substantial losses in human life, property, and overall societal and economic stability. Consequently, an in-depth examination of meteorological drought is instrumental in enhancing our knowledge and understanding of various other drought typologies.

The meteorological drought index serves as an indispensable instrument for the monitoring, early warning, and quantitative assessment of drought severity. Prominent indices such as the Standardized Precipitation Index (SPI) [12–14], Standardized Precipitation Evapotranspiration Index (SPEI) [15–22], and the Palmer Drought Severity Index (PDSI) are extensively utilized in current drought studies [22–28]. Due to their distinct foundational backgrounds and drought-inducing factors, these indices vary in regional suitability. Consequently, the accurate analysis of regional drought characteristics hinges on the judicious selection of appropriate drought indices. The PDSI, introduced by Palmer in 1965 [29], represents a sophisticated meteorological drought index. It integrates a range of critical factors, including historical precipitation patterns, water supply–demand equilibrium, and both actual and potential evapotranspiration rates. Despite its comprehensive approach, the PDSI falls short in capturing the multi-dimensional characteristics of drought phenomena. In an enhancement to the original model, the self-calibrating Palmer Drought Severity Index (scPDSI) has been developed [23,30–35]. This advanced index dynamically adjusts PDSI parameters in response to specific climatic data from individual stations, thus offering a more tailored and effective tool for assessing local climate conditions [36]. Furthermore, the SPEI further broadens the scope by incorporating variables such as temperature and precipitation, addressing the multi-scale dimensions of drought, and providing a more holistic understanding than the SPI [37,38]. Acknowledging the intricate genesis and diverse factors influencing drought, our study extensively employs both scPDSI and SPEI indices to meticulously investigate the spatial and temporal dynamics of drought within the designated study region.

In conventional methodologies, drought indices are often derived from meteorological station data or through interpolation within a specified region, a process that can introduce discontinuities at the boundaries. Addressing this limitation, this study not only investigates drought issues in the target area through remote sensing techniques but also innovates by selecting stations within designated buffer zones along the boundaries for refined interpolation. The Yellow River Basin (YRB) has a long-documented history of recurrent drought episodes, significantly impinging on the subsistence environment of its local populace. These drought events have precipitated a suite of detrimental outcomes, encompassing the diminution of agricultural output, cessation of river flows, and degradation of ecological systems. Collectively, these issues have emerged as principal constraints, impeding the trajectory of sustainable economic and societal advancement in the region. Given the recurring nature of droughts in the YRB, a thorough examination of these phenomena is imperative. The research objectives of this paper are (1) to conduct a detailed evaluation of the spatiotemporal dynamics of drought within the YRB; and (2) to perform an in-depth comparative analysis of the SPEI and scPDSI drought indices, assessing their efficacy in precisely depicting the drought characteristic of this vital geographical area.

2. Data and Methods

2.1. Study Area

The Yellow River, which has a total length of 5464 km and is the second-longest river in China after the Yangtze River and the fifth-longest river in the world, arises from the Bayankala Mountains in Qinghai Province, China [39,40]. The YRB is located between 96° and 119° east longitude and 32° and 42° north latitude, with a length of about 1900 km from east to west and a width of about 1100 km from north to south. The YRB is in the mid-latitude zone, where atmospheric circulation and monsoon circulation have a relatively complicated impact (as depicted in Figure 1). As a result, there are significant differences in climate between the basin's various regions, as well as significant annual and seasonal changes in climate elements. The YRB experiences dry winters and springs marked by drought and rainy summers and autumns, with precipitation from June to September making up roughly 70% of the entire year's total and precipitation from July to August in the summer exceeding 40% of the total. The drought situation in the YRB has become increasingly serious in recent years, severely restricting the sustainable development of the economy and society; therefore, analyzing the drought occurrence and development pattern in the YRB is of great significance in strengthening regional drought monitoring and management and promoting the ecological protection and high-quality development of the YRB. Table 1 presents the designations and corresponding abbreviations for the various sub-regions within the YRB.

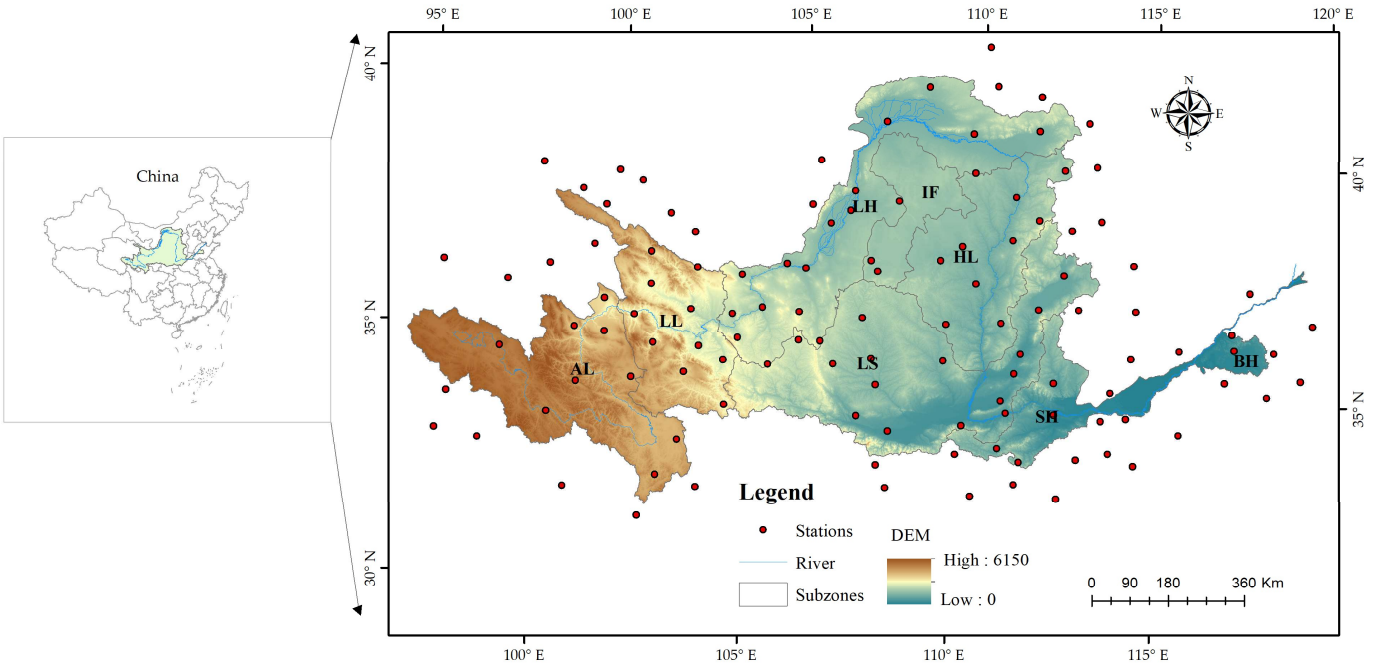

Figure 1. Location of the study area and distribution of meteorological stations.

Table 1. Sub-regions of the YRB.

Subzones	
above Longyangxia (AL)	inward flowing (IF)
Longyangxia to Lanzhou (LL)	Longmen to Sanmenxia (LS)
Lanzhou to Hekou (LH)	Sanmenxia to Huayuankou (SH)
Hekou to Longmen (HL)	below Huayuankou (BH)

2.2. Data

The selected meteorological dataset comprises monthly-scale observations from 120 meteorological stations across the Yellow River Basin and its surrounding areas, spanning the period from 1961 to 2017. This dataset includes parameters such as rainfall, average air temperature, maximum air temperature, minimum air temperature, wind speed, and sunshine hours. Self-calibrating Palmer Drought Severity Index (scPDSI) data were obtained from the Koninklijk Netherlands Meteorological Institute (KNMI) website of the Climate Research Unit (CRU) (http://climexp.knmi.nl/select.cgi?id=someone@somewhere&field=scpdsi (accessed on 12 June 2023)), which is globally gridded at a spatial resolution of 0.5°. Moreover, in the discussion section, the utilized SPEI dataset, characterized by a 3-month temporal resolution, is derived from the SPEI global database (SPEIbase). This repository furnishes comprehensive and dependable insights into global drought conditions, featuring a spatial resolution of 0.5 degrees and a temporal update frequency of once per month. The database encompasses a broad spectrum of SPEI temporal scales, varying from 1 to 48 months, thereby facilitating a nuanced understanding of drought dynamics over varying periods (http://climexp.knmi.nl/ (accessed on 18 June 2023)).

2.3. Methodology

2.3.1. Standardized Precipitation Evapotranspiration Index (SPEI)

In this study, the SPEI and PDSI drought indices were used to jointly investigate the drought conditions in the YRB, respectively. Vicente-Serrano et al. (2010) enhanced the SPI drought index by incorporating the potential evapotranspiration element, thereby developing the SPEI, which is adept at providing a precise representation of meteorological drought conditions [19]. In the computation of the SPEI, the prevailing methodologies for estimating potential evapotranspiration are the Thornthwaite and Penman–Monteith equations [41–49]. While the Thornthwaite approach, predominantly based on temperature, is extensively utilized in the existing literature, it offers a limited scope. The Penman–Monteith formula, in contrast, presents a more holistic approach by integrating both thermal and aerodynamic factors, thus providing a comprehensive assessment of potential evapotranspiration. This study, therefore, adopts the Penman–Monteith equation, recognizing its superior capacity to capture complex climatic interactions. The SPEI is then meticulously calculated, focusing on the extent to which the difference between the potential evapotranspiration and precipitation, as derived from the Penman–Monteith method, deviates from the mean state. This approach enables a detailed evaluation of the drought distribution characteristics, offering insights into its hydro-meteorological dynamics. Table 2 delineates the delineation criteria for various drought categories as defined by the SPEI and scPDSI indices [50,51].

Table 2. Categorization of Drought Severity Using SPEI and scPDSI Indices.

Drought Category	SPEI	scPDSI
No Drought	>-0.5	>-1.0
Mild Drought	$(-1.0, -0.5]$	$(-2.0, -1.0]$
Moderate Drought	$(-1.5, -1.0]$	$(-3.0, -2.0]$
Severe Drought	$(-2.0, -1.5]$	$(-4.0, -3.0]$
Extreme Drought	≤ -2.0	≤ -4.0

2.3.2. Self-Calibrating Palmer Drought Severity Index (scPDSI)

Palmer (1965) developed the PDSI drought index, which is based on the theory of water balance and takes past precipitation, soil water, runoff, and evapotranspiration processes into consideration [29]. Wells et al. (2004) developed the scPDSI by incorporating an automatic correction procedure for the persistence and climate weighting factors in the PDSI construction [36]. This resulted in a scPDSI that is site-specific and improves the PDSI's sensitivity to various wet and dry spaces. In order to achieve drought early

warning and disaster prevention and mitigation under changing environments, it is crucial to combine scPDSI, which is more applicable in different climate regimes, and SPEI, which has multi-time scale characteristics, to jointly analyze and identify the drought status and drought events, etc., in the YRB. In this study, we employ the metric of drought frequency to evaluate the prevalence of drought occurrences in the Yellow River Basin. Drought frequency is quantitatively defined as the proportion of the total time period during which drought conditions are observed within a specific region. The methodology for its computation is articulated as follows:

$$F = \frac{t}{T} \times 100\% \quad (1)$$

In the aforementioned equation, F denotes the drought frequency, quantified as a percentage (%); t signifies the temporal extent of drought occurrences; and T represents the aggregate duration under consideration.

2.3.3. Methodology for Trend Detection

The Modified Mann–Kendall (MMK) trend test represents a significant advancement over the conventional Mann–Kendall method. This refined approach adeptly mitigates the influence of autocorrelation within data series, thereby markedly augmenting the test's analytical prowess [52]. As a robust non-parametric methodology, MMK is exceptionally adept at discerning underlying trends within time series data. Its efficacy and versatility have led to its widespread adoption, particularly in the realms of hydrology and meteorology, where it has become a cornerstone tool for time series analysis. In light of its analytical robustness, this study opts for the MMK method to conduct trend analysis. For a detailed understanding of the computational procedures, readers are referred to the methodologies outlined in the relevant literature [53,54].

3. Results

3.1. Drought Assessment Based on the SPEI Index

SPEI can be calculated over different time scales, reflecting short-term and long-term moisture conditions. Figure 2 presents the interannual variability of SPEI values across various temporal scales within the YRB, specifically at 1-month, 3-month, 6-month, 12-month, and 24-month intervals. The blue bars represent SPEI values greater than 0, while the red bars indicate SPEI values less than 0. The graphical representation indicates a trend of diminishing fluctuation amplitudes with increasing temporal scales. Shorter time scales, ranging from 1 to 3 months, are predominantly indicative of vegetation's immediate response to hydric stress, which is critically relevant to agricultural practices as such short-term drought conditions can significantly impact crop productivity. The intermediate time scales of 3 to 6 months strike a balance by capturing the influences of both precipitation and temperature fluctuations. In contrast, scales extending to 12 months and beyond are demonstrative of the prolonged effects of drought, contributing to a more comprehensive understanding of the overarching drought trends. Utilizing the SPEI-12 on an annual scale, years with values below -0.5 are identified as experiencing drought. Accordingly, drought events were recorded in 1965, 1966, 1969, 1972, 1986, 1997, 1999, 2001, and 2006. Notably, the drought of 1997 emerged as the most severe, with 1965 following in severity.

In order to investigate the spatial and temporal characteristics of drought frequency within the YRB, this study computes the drought frequencies of various magnitudes using the SPEI-3 derived from regional meteorological stations. Subsequently, the kriging interpolation technique is employed to map and analyze the variations in drought frequency across the entirety of the YRB (as shown in Figure 3). The figure illustrates that the drought frequency variation within the YRB spans from 31% to 34%. Interpolation results indicate that the frequency in the LL region is comparatively higher, suggesting a relatively stable pattern of minimal fluctuation throughout the area.

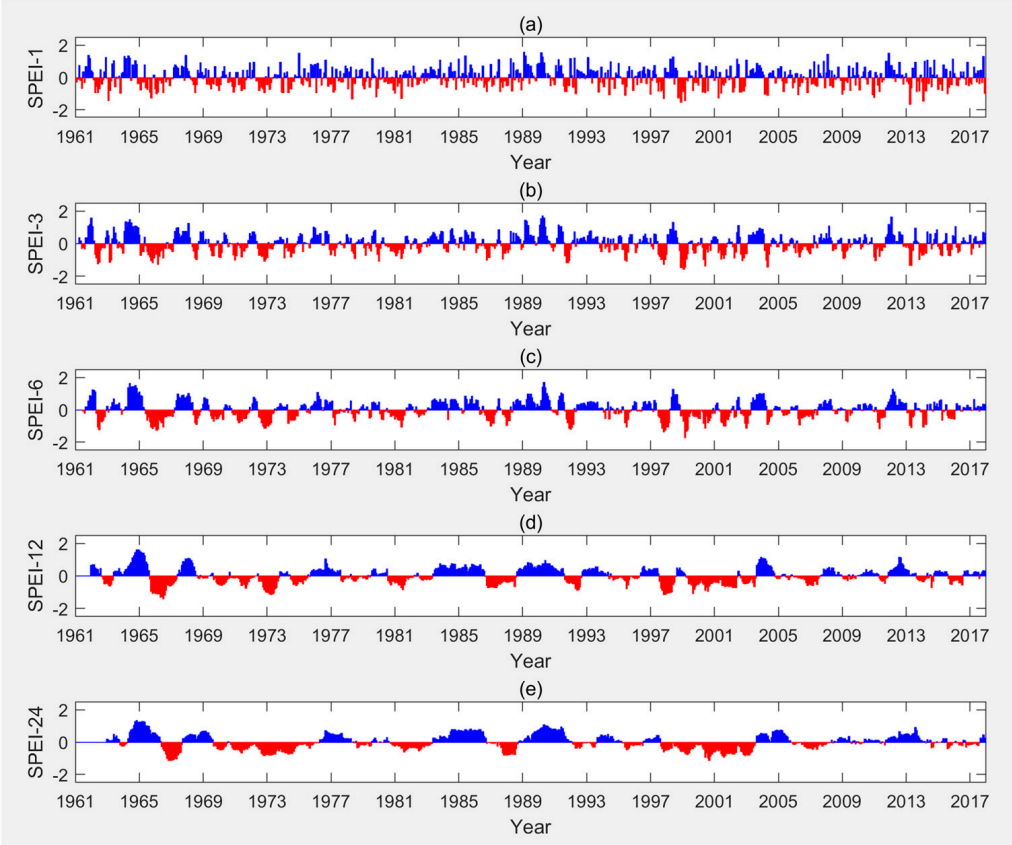

Figure 2. SPEI temporal sequences derived from meteorological station data at different time scales (blue signifying SPEI values above 0, red denoting SPEI values below 0): (**a**) 1-month scale; (**b**) 3-month scale; (**c**) 6-month scale; (**d**) 12-month scale; (**e**) 24-month scale.

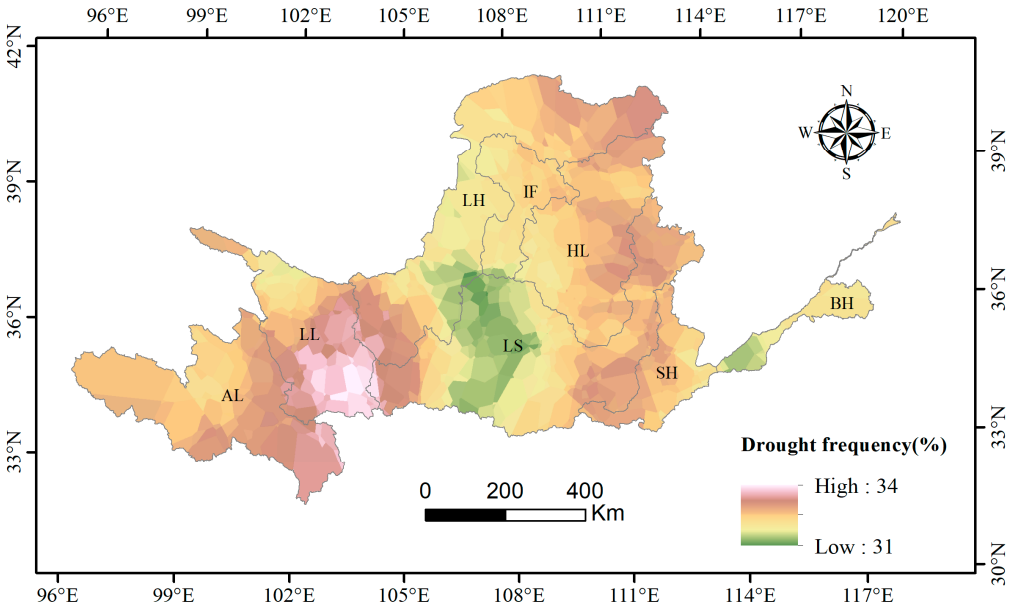

Figure 3. Assessment of drought frequency in the YRB derived from SPEI values on a 3-month temporal scale.

In order to more precisely determine the distribution characteristics of drought levels across various regions, we analyzed the mean drought grades recorded at meteorological stations within each respective subzone, as demonstrated in Figure 4. The distinctive characteristics associated with varying drought levels are depicted in the accompanying figure. The analysis presented in the figure indicates that, based on the average values derived from meteorological stations within each respective subzone, the BH region exhibits the highest incidence of drought frequency, followed by the LL region, whereas the IF region demonstrates the lowest frequency. In summary, each area predominantly experiences mild droughts, with frequencies ranging between 14.91% and 16.23%. Moderate droughts occur with the next highest frequency. In contrast, the occurrences of the other two drought severity levels are comparatively lower, particularly for extreme droughts, which manifest at a rate of approximately 1%.

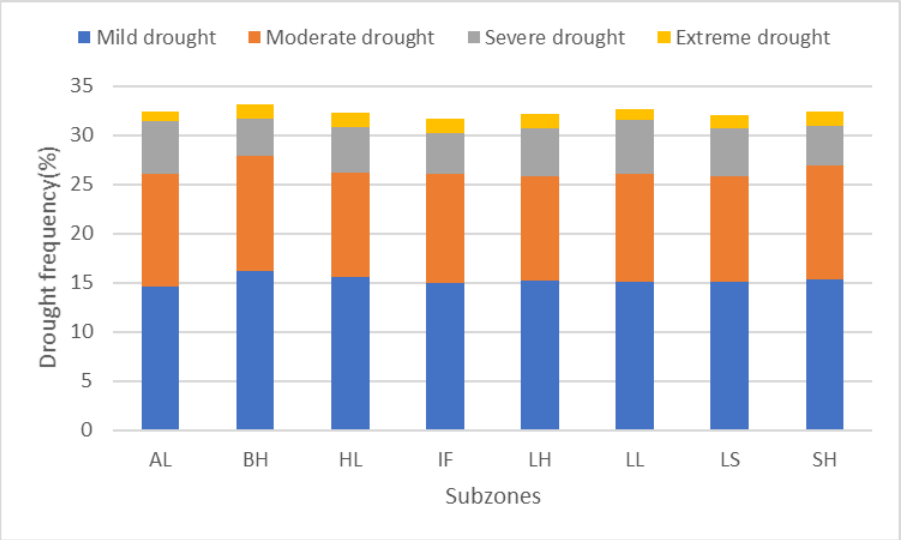

Figure 4. Characterization of the distribution of diverse drought frequencies across sub-regions in the YRB.

3.2. scPDSI-Based Drought Analysis

Figure 5 illustrates the variation in drought distribution across the YRB as determined by the scPDSI. It represents the mean scPDSI values calculated for each quarter and annually over an extended period from 1961 to 2017. On the seasonal scale, the YRB exhibits relatively uniform mean scPDSI values across different seasons: −0.98 in spring, −1.04 in summer, −1.06 in autumn, and −1.01 in winter. This indicates a negligible variation in the seasonal mean values of SPEI within the basin. The scPDSI values for each district were acquired by calculating the mean value of the scPDSI on an annual basis for each subzone: LH: −1.06; HL: −0.87; IF: −0.94; LS: −0.96; LL: −1.35; BH: −0.71; SH: −1.44; AL: −1.06. Based on the analysis of statistical average values, the SH and LL regions are notably more arid in comparison. However, when viewed on an annual scale, the HL, IF, LS, and BH regions exhibit no significant signs of drought conditions.

A Modified Mann–Kendall (MMK) trend test is utilized to analyze the trend of drought conditions in the YRB. The occurrence of positive values in the data signifies a trend towards increased humidity, whereas negative values are indicative of a shift towards more arid conditions. The analysis becomes notably significant when the absolute value of the Z-score surpasses thresholds of 1.65, 1.96, and 2.58, corresponding to the trend successfully meeting the criteria for significance at confidence intervals of 90%, 95%, and 99%, respectively. This indicates a robust and reliable understanding of the drought trends at these confidence levels. Employing a MMK trend analysis, this study presents a detailed spatiotemporal mapping of the monthly gridded drought trends within the YRB, as demonstrated in Figure 6. The resultant maps, illustratively depicted in the subsequent figures, encapsulate

the trends from January to December. A rigorous statistical approach was applied to calculate the mean values of the trend characteristics for each month, utilizing the scPDSI as the reference metric. The computed MMK trend characteristic values were as follows: −1.25 in January, −1.16 in February, −1.27 in March, −1.41 in April, −1.11 in May, −0.97 in June, −1.28 in July, −1.45 in August, −1.23 in September, −1.08 in October, −1.15 in November, and −1.08 in December. The uniformly negative values across all months robustly indicate a consistent downward trajectory in the PDSI. This finding signifies an alarming, yet statistically significant, trend towards escalating drought conditions within the YRB, warranting immediate attention and action in the context of regional water resource management and climate adaptation strategies.

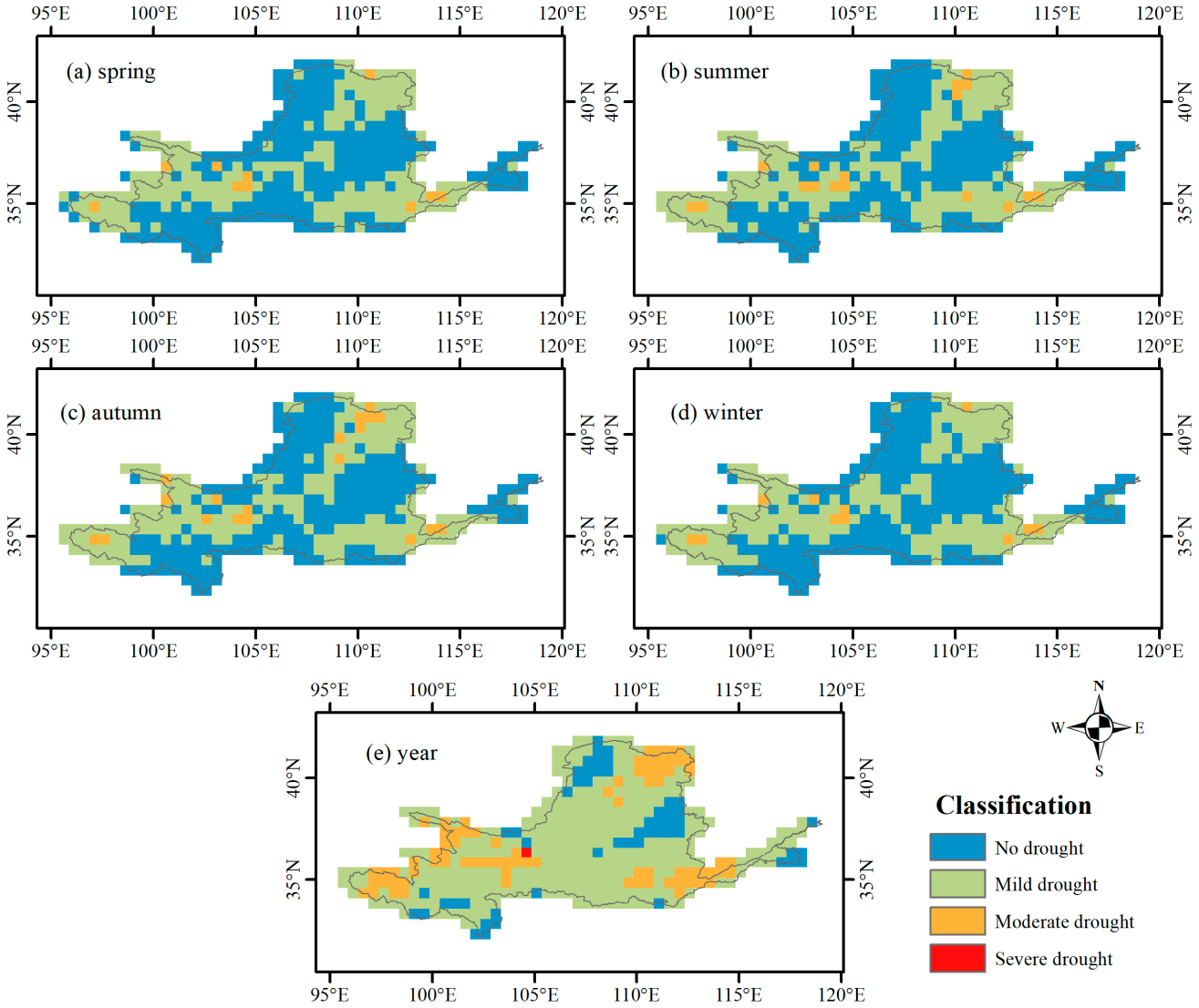

Figure 5. Spatial distribution of varied drought intensities, according to the average scPDSI values from the 1961–2017 time series: (**a**) spring season; (**b**) summer season; (**c**) autumn season; (**d**) winter season; (**e**) annual mean.

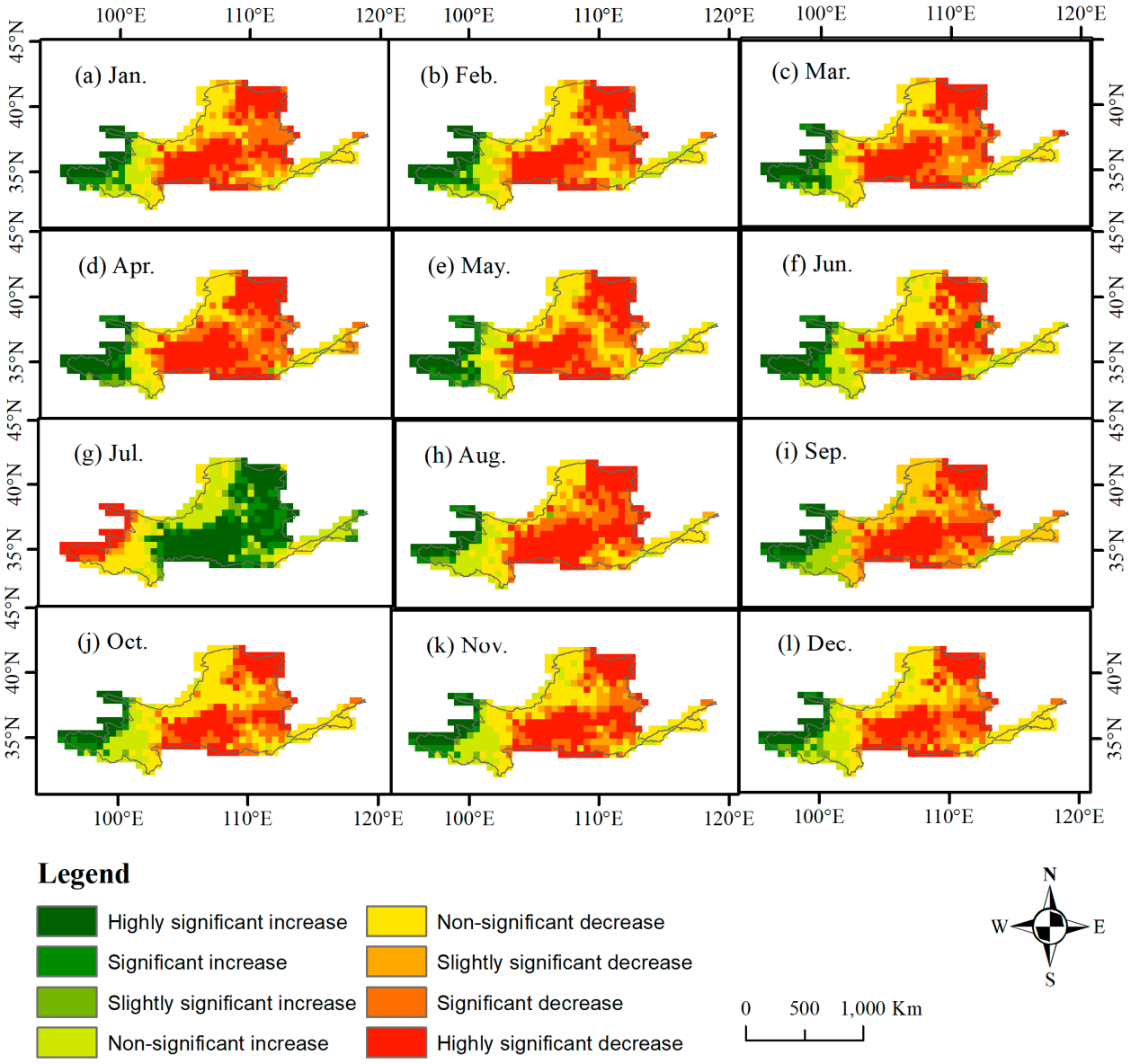

Figure 6. Trend analysis of the YRB: evaluating scPDSI values from 1961 to 2017.

3.3. Comparative Evaluation of Two Drought Indices

In this study, we conduct an advanced analysis of the drought dynamics within the YRB, utilizing two sophisticated meteorological drought indices. The SPEI is employed, offering a holistic approach that integrates critical climatic factors, notably precipitation and temperature. SPEI is able to encapsulate multiple temporal scales, providing a nuanced understanding of drought patterns. In contrast, the scPDSI is also applied, which comprehensively accounts for variables such as antecedent precipitation, potential evapotranspiration, and soil moisture content. Therefore, both indices are used to analyze the drought conditions in the YRB.

In this research, we executed a correlation analysis juxtaposing the scPDSI with the SPEI across diverse temporal scales, 1 month, 3 months, 6 months, 12 months, and 24 months, as illustrated in Figure 7. Both of these drought indices corroborate the occurrence of a significant drought event within the YRB in 1997, aligning with the observed realities. The year 1997 marked the onset of the most profound drought recorded in the basin's history, characterized by the lowest annual precipitation levels and sustained elevated temperatures across vast swathes of the region. The derived correlation coefficients (r) were found to be 0.35, 0.54, 0.69, 0.76, and 0.62 for each respective time scale, as illus-

trated in the figure. These findings elucidate that the correlation is comparatively weakest on the 1-month scale. Conversely, the correlation reaches its zenith on an annual basis. This pattern is sequentially followed in terms of strength by the 6-month, 24-month, and 3-month intervals. Such results offer insightful implications for understanding the temporal dynamics of drought severity and their interactions with varying climatic indices. The concurrent utilization of both indices in this research offers a comprehensive and detailed analysis of the drought conditions prevalent in the YRB, paving the way for more informed water resource management and climate resilience strategies in this crucial geographic region.

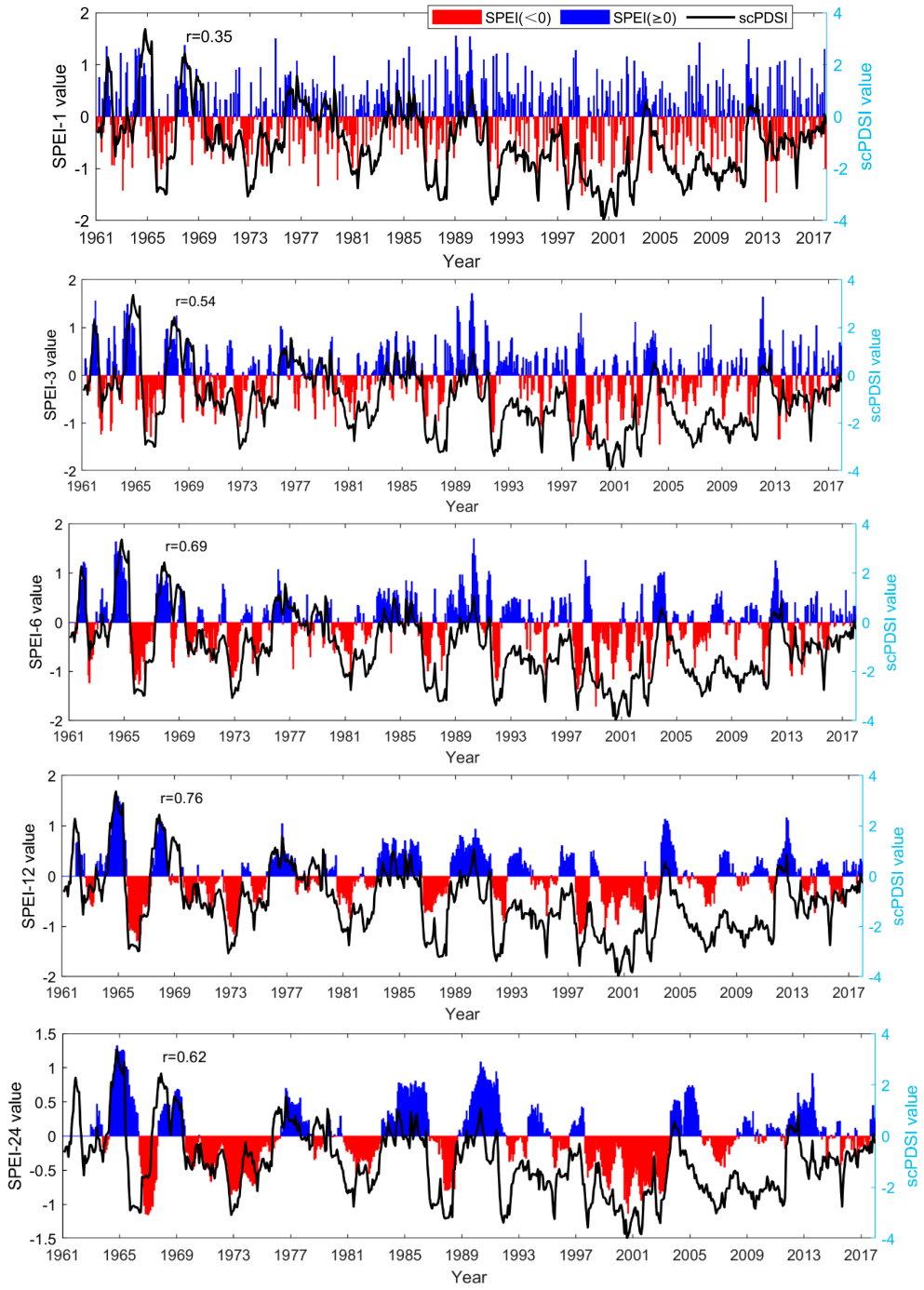

Figure 7. Comparative time series analysis of SPEI (blue and red bars) and scPDSI (black solid line) values across various time scales: a study from 1961 to 2017.

In an effort to conduct a more nuanced comparative analysis of the capabilities of the SPEI and scPDSI drought indices in representing drought characteristics within the YRB, this study involved the construction of correlation plots between various scales of SPEI and scPDSI across numerous stations. Subsequently, we employed kriging interpolation on these station-specific correlations to produce a comprehensive map. The analysis revealed distinct correlation ranges between the indices at different scales: the correlation between SPEI-1 and scPDSI was found to be between 0.23 and 0.36 (as depicted in Figure 8a); for SPEI-3 and scPDSI, it ranged from 0.24 to 0.52 (Figure 8b); for SPEI-6 and scPDSI, it showed a correlation spread from 0.37 to 0.63 (Figure 8c); for SPEI-12 and scPDSI, it extended from 0.40 to 0.67 (Figure 8d); and, finally, SPEI-24 and scPDSI exhibited a correlation range of 0.25 to 0.66 (Figure 8e). The aforementioned findings reveal that, according to the station-based correlation charts, the greatest correlation is observed at a 12-month time scale across various temporal ranges, followed sequentially by 6 months and 24 months. This pattern underscores the suitability of scPDSI for monitoring medium- to long-term drought phenomena, a characteristic attributable to its inherent lagged autocorrelation properties. Zhao et al. [55] conducted a comprehensive analysis of the temporal scale differences between scPDSI and SPEI in the context of drought monitoring across various Chinese regions. Their findings revealed that the maximum correlation between scPDSI and SPEI, specifically over a period ranging from 9 to 19 months, was observed across diverse geographical areas. This observation is in concordance with the results delineated in the current study, reinforcing the robustness and consistency of these findings within the broader research landscape.

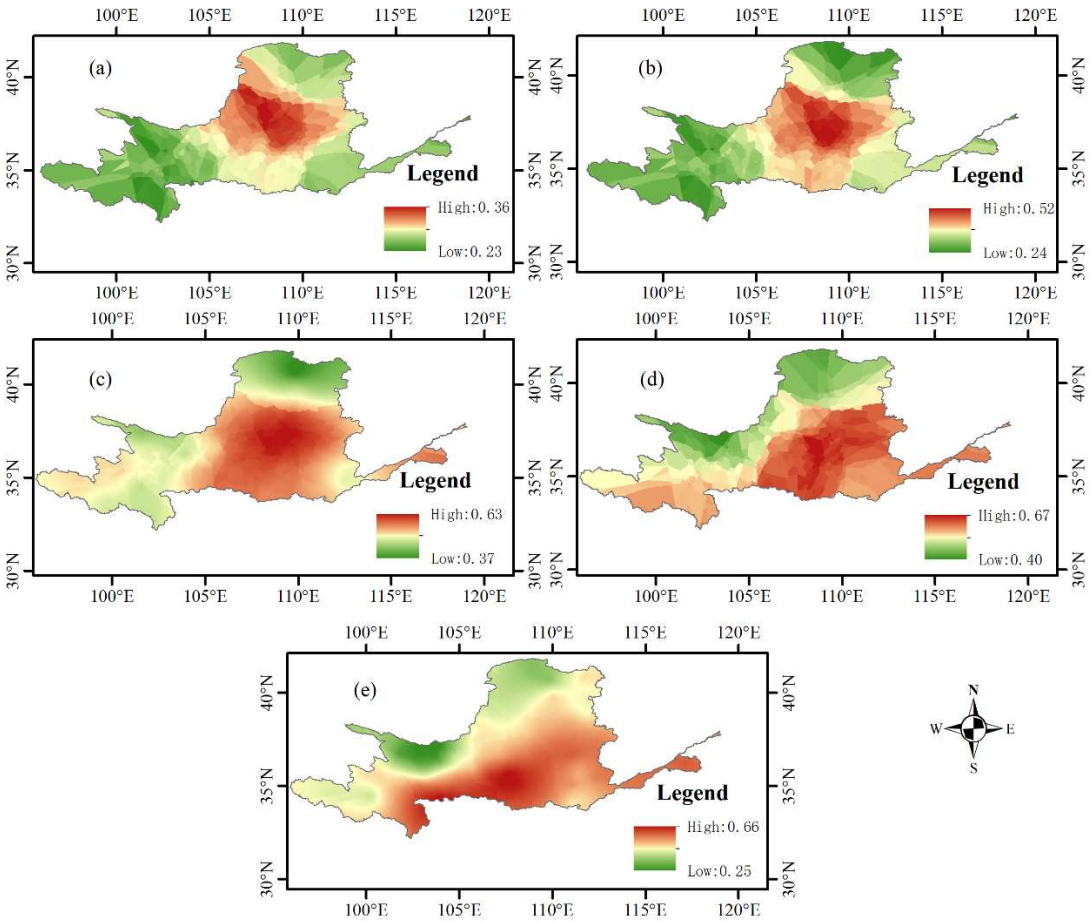

Figure 8. Kriging interpolation analysis of the correlation between meteorological station-based SPEI and scPDSI across various temporal scales: (**a**) 1-month scale; (**b**) 3-month scale; (**c**) 6-month scale; (**d**) 12-month scale; (**e**) 24-month scale.

To gain a more comprehensive understanding of the correlations within diverse sub-regions, we calculated the average correlations for each sub-region, drawing from the data illustrated in the preceding chart, and synthesized these findings into Figure 9. This meticulous analysis uncovers a significant correlation between SPEI-12 and scPDSI, highlighting a notable interconnection. Moreover, when examining across varied temporal scales, it becomes apparent that certain sub-regions, namely LS, IF, HL, and BH, exhibit remarkably robust correlations. This insight is of paramount importance for the strategic formulation of bespoke drought mitigation strategies in these specific sub-regions. Such strategies are aimed at substantially diminishing the prevalence of drought-induced calamities and simultaneously bolstering the overall capacity for a more effective and responsive adaptation to these environmental challenges.

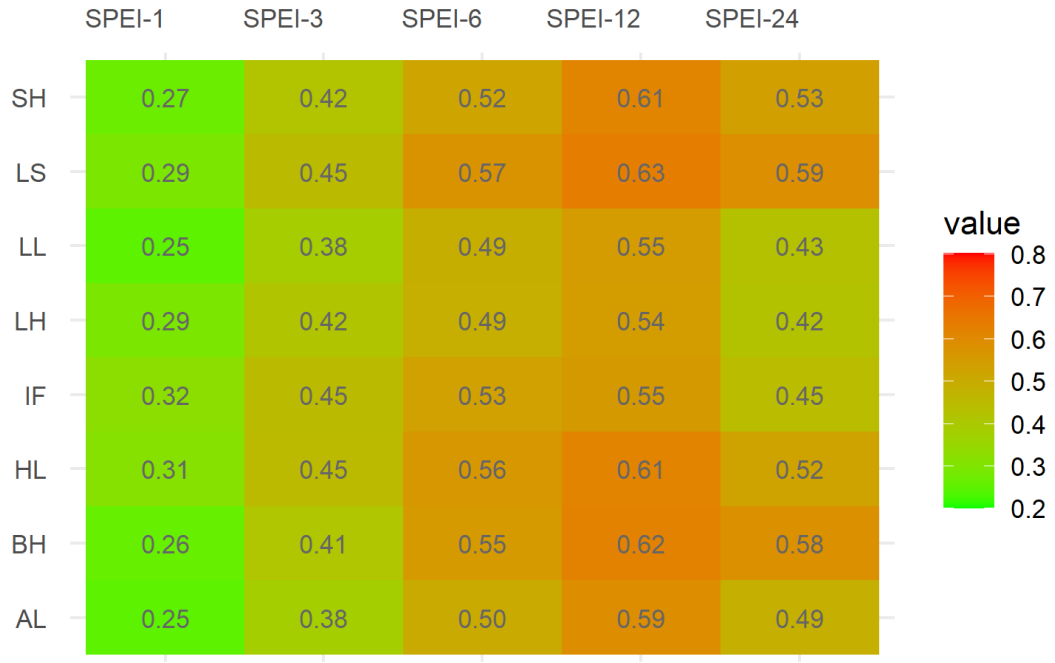

Figure 9. Analyzing the distribution of correlation coefficients (r) between SPEI and scPDSI across temporal scales in diverse sub-regions of the YRB.

4. Discussion

Although interpolation analysis on the station-based SPEI values was conducted earlier in our study, it is important to note that such interpolated outcomes are susceptible to variations induced by topographical features and spatial station distribution. To mitigate these effects and enhance the robustness of our analysis, we have conducted a comparative assessment, juxtaposing SPEI values calculated at station level with those derived from 0.5-degree-resolution gridded SPEI datasets over a temporal scale of 3 months. Figure 10 presents the time series analysis of SPEI values computed from station data juxtaposed with those obtained from gridded datasets, spanning from 1961 to 2017 in the YRB. The depicted correlation coefficient of 0.93 signifies a robust congruence between the two datasets, substantiating the efficacy of gridded SPEI values in capturing the hydrological dynamics of the region. This high fidelity suggests that gridded SPEI data are well suited for future evaluations of drought conditions within the basin.

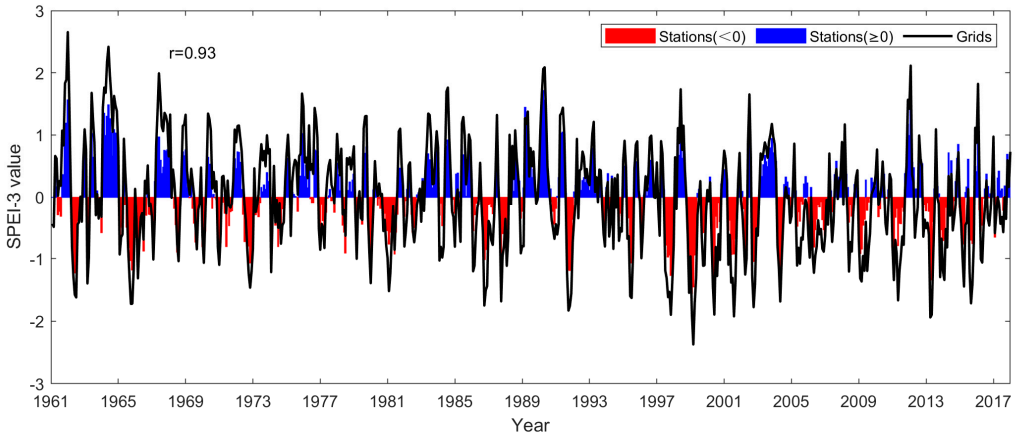

Figure 10. Temporal dynamics of station-derived versus gridded SPEI values in the YRB, 1961–2017.

Following the temporal series analysis of SPEI values computed from station-based measurements versus gridded datasets, we sought to elucidate the spatial applicability of gridded data within our study domain. This involved leveraging station data to extract corresponding values from the gridded dataset at precise locations. Correlation coefficients were then calculated for each station in relation to its respective gridded data point. Employing the kriging interpolation technique, this process culminates in Figure 11, which illustrates the spatial correlation of gridded SPEI data across the study area. The analysis depicted in Figure 11 reveals a discernible spatial gradient in correlation levels, extending from the northwest towards the southeast, with an increasing trend in correlation coefficients that range between 0.61 and 0.88. Within the delineated sub-regions of the study area, the correlation levels are ranked as follows: BH (0.865) > SH (0.858) > LS (0.845) > HL (0.817) > IF (0.749) > LH (0.736) > AL (0.729) > LL (0.713). This demonstrates a commendable degree of correlation between the Standardized Precipitation Evapotranspiration Index (SPEI) values derived from station data and those obtained from grid-based datasets. Consequently, for subsequent drought assessments at the grid scale, grid-based data emerge as a viable analytical resource. Nevertheless, it is pertinent to note that the resolution of grid data currently prevalent for drought assessments is comparatively coarse, necessitating enhancements for precise evaluations in smaller catchments or scenarios demanding higher resolution data.

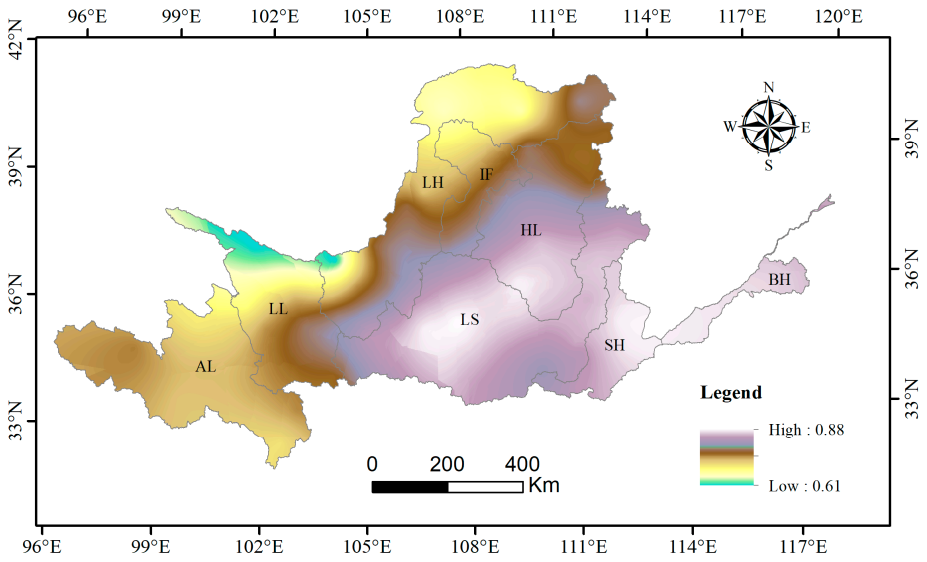

Figure 11. Spatial interpolation analysis of the correlation between station-derived and grid-based SPEI values in the YRB.

5. Conclusions

Most of the YRB is located in the arid and semi-arid regions of China, characterized by a fragile ecological environment that supports a vast economic scale and a large population. Therefore, analyzing the patterns of drought occurrence and development in the YRB under changing environmental conditions is of significant importance for enhancing regional drought monitoring and management and for promoting ecological protection and high-quality development in the basin. In this study, the YRB is the research subject, employing the meteorological drought indices SPEI and scPDSI to analyze the spatiotemporal variations in drought conditions. It delves into the utility of SPEI and scPDSI for effective drought monitoring in the basin, providing a comprehensive and methodical exploration of the drought's spatiotemporal dynamics. The following conclusions were drawn:

(1) The SPEI demonstrates distinct fluctuation patterns at varying temporal scales, with shorter scales exhibiting more pronounced amplitude variations. An analysis of drought occurrences through SPEI over these scales highlights several critical drought years in the YRB, specifically 1965, 1966, 1969, 1972, 1986, 1997, 1999, 2001, and 2006. Furthermore, when the SPEI is computed on a three-month time scale, it reveals that the frequency of drought events in the basin oscillates between 31% and 34%, underscoring the variability and intensity of drought conditions within this region.

(2) In our study, the MMK trend test was applied to the scPDSI time series, revealing a concerning upward trend in the severity of drought conditions across the YRB. Furthermore, the regional scPDSI values were derived from the calculation of mean annual scPDSI values for each sub-region, yielding the following: LH: −1.06; HL: −0.87; IF: −0.94; LS: −0.96; LL: −1.35; BH: −0.71; SH: −1.44; AL: −1.06. These figures notably highlight the regions of SH and LL as experiencing markedly more severe drought conditions.

(3) A comprehensive correlation analysis was carried out between scPDSI and SPEI across multiple temporal scales, including 1 month, 3 months, 6 months, 12 months, and 24 months. This analysis yielded correlation coefficients (r) of 0.35, 0.54, 0.69, 0.76, and 0.62, respectively. These findings underscore a significant insight: the correlation between scPDSI and SPEI reaches its apex on an annual scale, whereas it is relatively minimal on a monthly scale. The correlation analysis of SPEI and scPDSI across different scales in spatial terms indicates that, within various temporal extents, the 12-month time scale exhibits the highest correlation, followed by 6 months and 24 months. This pattern underscores the suitability of scPDSI for monitoring medium- to long-term drought phenomena, a characteristic attributed to its inherent lag autocorrelation properties.

Author Contributions: Conceptualization, L.J. and S.C.; methodology, L.J.; software, S.C. and M.L.; validation, S.C. and M.L.; formal analysis, L.J.; investigation, S.C.; resources, S.C.; data curation, L.J.; writing—original draft preparation, L.J.; writing—review and editing, S.C.; visualization, L.J. and M.L.; supervision, S.C.; project administration, S.C.; funding acquisition, S.C. All authors have read and agreed to the published version of the manuscript.

Funding: This research was funded by the Natural Science Foundation of Henan Province (No. 222300420317) and the National Key Research and Development Program of China (No. 2021YFC3200201).

Data Availability Statement: All the data that supports the findings of this study is included in the article, and the raw data can be obtained through a public web site. The meteorological data used in this study are confidential.

Acknowledgments: Thanks to the Koninklijk Netherlands Meteorological Institute (KNMI) website of the Climate Research Unit (CRU) for offering Self-calibrating Palmer Drought Severity Index (scPDSI) data (http://climexp.knmi.nl/select.cgi?id=someone@somewhere&field=scpdsi (accessed on 12 June 2023)) and the SPEI dataset (http://climexp.knmi.nl/ (accessed on 18 June 2023)). Sincere thanks are due to the editor and the anonymous reviewers for all the remarks and suggestions that were very helpful and constructive for improving our manuscript.

Conflicts of Interest: The authors declare no conflicts of interest.

References

1. Chen, Z.H.; Yang, G.F. Analysis of drought hazards in North China: Distribution and interpretation. *Nat. Hazards* **2013**, *65*, 279–294. [CrossRef]
2. Zhao, Z.Y.; Hao, X.M.; Fan, X.; Zhang, J.J.; Zhang, S.; Li, X.W. Actual Evapotranspiration Dominates Drought in Central Asia. *Remote Sens.* **2023**, *15*, 4557. [CrossRef]
3. Naidoo, S. Commentary on the contribution of Working Group III to the Sixth Assessment Report of the Intergovernmental Panel on Climate Change. *S. Afr. J. Sci.* **2022**, *118*, 1–4. [CrossRef] [PubMed]
4. Zhang, J.W.; Wang, J.G.; Chen, S.B.; Wang, M.C.; Tang, S.Q.; Zhao, W.T. Integrated Risk Assessment of Agricultural Drought Disasters in the Major Grain-Producing Areas of Jilin Province, China. *Land* **2023**, *12*, 160. [CrossRef]
5. Mukherjee, S.; Mishra, A.; Trenberth, K.E. Climate Change and Drought: A Perspective on Drought Indices. *Curr. Clim. Chang. Rep.* **2018**, *4*, 145–163. [CrossRef]
6. Esfahanian, E.; Nejadhashemi, A.P.; Abouali, M.; Adhikari, U.; Zhang, Z.; Daneshvar, F.; Herman, M.R. Development and evaluation of a comprehensive drought index. *J. Environ. Manag.* **2017**, *185*, 31–43. [CrossRef]
7. Sheffield, J.; Wood, E.F.; Roderick, M.L. Little change in global drought over the past 60 years. *Nature* **2012**, *491*, 435–438. [CrossRef]
8. Spinoni, J.; Barbosa, P.; Bucchignani, E.; Cassano, J.; Cavazos, T.; Christensen, J.H.; Christensen, O.B.; Coppola, E.; Evans, J.; Geyer, B.; et al. Future Global Meteorological Drought Hot Spots: A Study Based on CORDEX Data. *J. Clim.* **2020**, *33*, 3635–3661. [CrossRef]
9. Haile, G.G.; Tang, Q.; Li, W.; Liu, X.; Zhang, X. Drought: Progress in broadening its understanding. *Wiley Interdiscip. Rev. Water* **2020**, *7*, e1407. [CrossRef]
10. Zhao, M.; Huang, S.; Huang, Q.; Wang, H.; Leng, G.; Xie, Y. Assessing socio-economic drought evolution characteristics and their possible meteorological driving force. *Geomat. Nat. Hazards Risk* **2019**, *10*, 1084–1101. [CrossRef]
11. Bachmair, S.; Stahl, K.; Collins, K.; Hannaford, J.; Acreman, M.; Svoboda, M.; Knutson, C.; Smith, K.H.; Wall, N.; Fuchs, B. Drought indicators revisited: The need for a wider consideration of environment and society. *Wiley Interdiscip. Rev. Water* **2016**, *3*, 516–536. [CrossRef]
12. Chen, S.; Muhammad, W.; Lee, J.-H.; Kim, T.-W. Assessment of Probabilistic Multi-Index Drought Using a Dynamic Naive Bayesian Classifier. *Water Resour. Manag.* **2018**, *32*, 4359–4374. [CrossRef]
13. Sian, K.T.C.L.K.; Zhi, X.; Ayugi, B.O.; Onyutha, C.; Shilenje, Z.W.; Ongoma, V. Meteorological Drought Variability over Africa from Multisource Datasets. *Atmosphere* **2023**, *14*, 1052. [CrossRef]
14. Xu, Z.; Wu, Z.; Shao, Q.; He, H.; Guo, X. From meteorological to agricultural drought: Propagation time and probabilistic linkages. *J. Hydrol.-Reg. Stud.* **2023**, *46*, 101329. [CrossRef]
15. Ayantobo, O.O.; Li, Y.; Song, S.; Yao, N. Spatial comparability of drought characteristics and related return periods in mainland China over 1961–2013. *J. Hydrol.* **2017**, *550*, 549–567. [CrossRef]
16. Khatiwada, K.R.; Pandey, V.P. Characterization of hydro-meteorological drought in Nepal Himalaya: A case of Karnali River Basin. *Weather Clim. Extrem.* **2019**, *26*, 100239. [CrossRef]
17. Wable, P.S.; Jha, M.K.; Shekhar, A. Comparison of Drought Indices in a Semi-Arid River Basin of India. *Water Resour. Manag.* **2019**, *33*, 75–102. [CrossRef]
18. Zhang, N.; Li, Z.; Quiring, S.M. Developing Impacts-Based Drought Thresholds for Ohio. *J. Hydrometeorol.* **2023**, *24*, 1225–1240. [CrossRef]
19. Vicente-Serrano, S.M.; Beguería, S.; López-Moreno, J.I. A Multiscalar Drought Index Sensitive to Global Warming: The Standardized Precipitation Evapotranspiration Index. *J. Clim.* **2010**, *23*, 1696–1718. [CrossRef]
20. Chen, J.; Zhang, B.; Zhou, J.; Guo, F. Temporal and Spatial Changes of Drought Characteristics in Temperate Steppes in China from 1960 to 2020. *Sustainability* **2023**, *15*, 12909. [CrossRef]
21. Sun, H.; Sun, X.; Chen, J.; Deng, X.; Yang, Y.; Qin, H.; Chen, F.; Zhang, W. Different types of meteorological drought and their impact on agriculture in Central China. *J. Hydrol.* **2023**, *627*, 130423. [CrossRef]
22. Xu, Y.; Zhu, X.; Cheng, X.; Gun, Z.; Lin, J.; Zhao, J.; Yao, L.; Zhou, C. Drought assessment of China in 2002–2017 based on a comprehensive drought index. *Agric. For. Meteorol.* **2022**, *319*, 108922. [CrossRef]
23. Yu, H.; Zhang, Q.; Xu, C.-Y.; Du, J.; Sun, P.; Hu, P. Modified Palmer Drought Severity Index: Model improvement and application. *Environ. Int.* **2019**, *130*, 104951. [CrossRef]
24. Ding, Y.; Xu, J.; Wang, X.; Peng, X.; Cai, H. Spatial and temporal effects of drought on Chinese vegetation under different coverage levels. *Sci. Total Environ.* **2020**, *716*, 137166. [CrossRef]
25. Ryu, J.H.; Sohrabi, M.; Acharya, A. Toward Mapping Gridded Drought Indices to Evaluate Local Drought in a Rapidly Changing Global Environment. *Water Resour. Manag.* **2014**, *28*, 3859–3869. [CrossRef]
26. Wu, B.; Ma, Z.; Yan, N. Agricultural drought mitigating indices derived from the changes in drought characteristics. *Remote Sens. Environ.* **2020**, *244*, 111813. [CrossRef]

27. Bazrkar, M.H.; Zhang, J.; Chu, X. Hydroclimatic aggregate drought index (HADI): A new approach for identification and categorization of drought in cold climate regions. *Stoch. Environ. Res. Risk Assess.* **2020**, *34*, 1847–1870. [CrossRef]
28. Yin, G.; Zhang, H. A new integrated index for drought stress monitoring based on decomposed vegetation response factors. *J. Hydrol.* **2023**, *618*, 129252. [CrossRef]
29. Palmer, W.C. *Meteorological Drought*; US Department of Commerce, Weather Bureau: Silver Spring, MD, USA, 1965; Volume 30.
30. Mi, Q.; Ren, C.; Wang, Y.; Gao, X.; Liu, L.; Li, Y. A robust ensemble drought index: Construction and assessment. *Nat. Hazards* **2023**, *116*, 1139–1159. [CrossRef]
31. Svoboda, M.D.; Fuchs, B.A.; Poulsen, C.C.; Nothwehr, J.R. The drought risk atlas: Enhancing decision support for drought risk management in the United States. *J. Hydrol.* **2015**, *526*, 274–286. [CrossRef]
32. Wang, H.; Vicente-serrano, S.M.; Tao, F.; Zhang, X.; Wang, P.; Zhang, C.; Chen, Y.; Zhu, D.; El Kenawy, A. Monitoring winter wheat drought threat in Northern China using multiple climate-based drought indices and soil moisture during 2000–2013. *Agric. For. Meteorol.* **2016**, *228*, 1–12. [CrossRef]
33. Zhang, R.; Qu, Y.; Zhang, X.; Wu, X.; Zhou, X.; Ren, B.; Zeng, J.; Wang, Q. Spatiotemporal variability in annual drought severity, duration, and frequency from 1901 to 2020. *Clim. Res.* **2022**, *87*, 81–97. [CrossRef]
34. Gobena, A.K.; Gan, T.Y. Assessment of Trends and Possible Climate Change Impacts on Summer Moisture Availability in Western Canada based on Metrics of the Palmer Drought Severity Index. *J. Clim.* **2013**, *26*, 4583–4595. [CrossRef]
35. van der Schrier, G.; Barichivich, J.; Briffa, K.R.; Jones, P.D. A scPDSI-based global data set of dry and wet spells for 1901–2009. *J. Geophys. Res.-Atmos.* **2013**, *118*, 4025–4048. [CrossRef]
36. Wells, N.; Goddard, S.; Hayes, M.J. A self-calibrating Palmer Drought Severity Index. *J. Clim.* **2004**, *17*, 2335–2351. [CrossRef]
37. Zeng, J.; Zhang, R.; Qu, Y.; Bento, V.A.; Zhou, T.; Lin, Y.; Wu, X.; Qi, J.; Shui, W.; Wang, Q. Improving the drought monitoring capability of VHI at the global scale via ensemble indices for various vegetation types from 2001 to 2018. *Weather Clim. Extrem.* **2022**, *35*, 100412. [CrossRef]
38. Dong, X.; Zhou, Y.; Liang, J.; Zou, D.; Wu, J.; Wang, J. Assessment of Spatiotemporal Patterns and the Effect of the Relationship between Meteorological Drought and Vegetation Dynamics in the Yangtze River Basin Based on Remotely Sensed Data. *Remote Sens.* **2023**, *15*, 3641. [CrossRef]
39. Huang, S.; Huang, Q.; Chang, J.; Zhu, Y.; Leng, G.; Xing, L. Drought structure based on a nonparametric multivariate standardized drought index across the Yellow River basin, China. *J. Hydrol.* **2015**, *530*, 127–136. [CrossRef]
40. Wang, F.; Wang, Z.; Yang, H.; Di, D.; Zhao, Y.; Liang, Q.; Hussain, Z. Comprehensive evaluation of hydrological drought and its relationships with meteorological drought in the Yellow River basin, China. *J. Hydrol.* **2020**, *584*, 124751. [CrossRef]
41. Abedi-Koupai, J.; Dorafshan, M.-M.; Javadi, A.; Ostad-Ali-Askari, K. Estimating potential reference evapotranspiration using time series models (case study: Synoptic station of Tabriz in northwestern Iran). *Appl. Water Sci.* **2022**, *12*, 212. [CrossRef]
42. Medeiros, P.V.; Noronha Marcuzzo, F.F.; Youlton, C.; Wendland, E. Error Autocorrelation and Linear Regression for Temperature-Based Evapotranspiration Estimates Improvement. *J. Am. Water Resour. Assoc.* **2012**, *48*, 297–305. [CrossRef]
43. Ahmadi, S.H.; Fooladmand, H.R. Spatially distributed monthly reference evapotranspiration derived from the calibration of Thornthwaite equation: A case study, South of Iran. *Irrig. Sci.* **2008**, *26*, 303–312. [CrossRef]
44. da Silva, V.J.; Carvalho, H.d.P.; da Silva, C.R.; de Camargo, R.; Franco Teodoro, R.E. Performance of Different Methods of Estimating the Daily Reference Evapotranspiration in Uberlandia, MG. *Biosci. J.* **2011**, *27*, 95–101.
45. Gharehbaghi, A.; Kaya, B. Calibration and evaluation of six popular evapotranspiration formula based on the Penman-Monteith model for continental climate in Turkey. *Phys. Chem. Earth* **2022**, *127*, 103190. [CrossRef]
46. Nguyen Dinh Giang, N.; Le Nhu, Y.; Lam Van, T.; Huynh Vuong Thu, M.; Kumar, P.; Nguyen Vo Chau, N. Evaluating Reference Crop Evapotranspiration of the Selected Field Crops Grown in Different Agricultural Regions in the Vietnamese Mekong Delta. *J. Clim. Chang.* **2022**, *8*, 1–12. [CrossRef]
47. Trajkovic, S. Temperature-based approaches for estimating reference evapotranspiration. *J. Irrig. Drain. Eng.* **2005**, *131*, 316–323. [CrossRef]
48. Trajkovic, S.; Gocic, M.; Pongracz, R.; Bartholy, J.; Milanovic, M. Assessment of Reference Evapotranspiration by Regionally Calibrated Temperature-Based Equations. *Ksce J. Civ. Eng.* **2020**, *24*, 1020–1027. [CrossRef]
49. Zhang, L.; Zhao, X.; Ge, J.; Zhang, J.; Traore, S.; Fipps, G.; Luo, Y. Evaluation of Five Equations for Short-Term Reference Evapotranspiration Forecasting Using Public Temperature Forecasts for North China Plain. *Water* **2022**, *14*, 2888. [CrossRef]
50. Yang, Q.; Li, M.; Zheng, Z.; Ma, Z. Regional applicability of seven meteorological drought indices in China. *Sci. China Earth Sci.* **2017**, *60*, 745–760. [CrossRef]
51. Han, X.; Wu, J.; Zhou, H.; Liu, L.; Yang, J.; Shen, Q.; Wu, J. Intensification of historical drought over China based on a multi-model drought index. *Int. J. Climatol.* **2020**, *40*, 5407–5419. [CrossRef]
52. Huang, S.; Chang, J.; Huang, Q.; Chen, Y. Spatio-temporal Changes and Frequency Analysis of Drought in the Wei River Basin, China. *Water Resour. Manag.* **2014**, *28*, 3095–3110. [CrossRef]
53. Wang, F.; Yang, H.; Wang, Z.; Zhang, Z.; Li, Z. Drought Evaluation with CMORPH Satellite Precipitation Data in the Yellow River Basin by Using Gridded Standardized Precipitation Evapotranspiration Index. *Remote Sens.* **2019**, *11*, 485. [CrossRef]

54. Huang, S.; Huang, Q.; Zhang, H.; Chen, Y.; Leng, G. Spatio-temporal changes in precipitation, temperature and their possibly changing relationship: A case study in the Wei River Basin, China. *Int. J. Climatol.* **2016**, *36*, 1160–1169. [CrossRef]
55. Zhao, H.Y.; Gao, G.; An, W.; Zou, X.L.; Li, H.T.; Hou, M.T. Timescale differences between SC-PDSI and SPEI for drought monitoring in China. *Phys. Chem. Earth* **2017**, *102*, 48–58. [CrossRef]